Supporting Information

Bandgap Engineering for Efficient Perovskite Solar Cells Under Multiple Color Temperature Indoor Lighting

Miqad S. Albishi [1+], Faisal I. Alabdulkarem[2+], George Perrakis[3+], Tariq F. Alhuwaymel[1+], Ala H. Sabeeh[4-5], Abdullah S. Alharbi[1], Naif R. Alshamrani[1], Ibrahim H. Khawaji[4-5], Nikolaos Tzoganakis[6], Majed M. Aljomah[1], Dimitris Tsikritzis[6], Sami A. Alhusaini[1], Abdullah Aljalalah[1], Kadi S. AlShebl[1], Ali Alanzi[1], Abrar Bin Ajaj[7], Fay M. Alotaibi[1], Hamad Albrithen[7-10] Konstantinos Petridis[8], Maria Kafesaki[3,9], Emmanuel Kymakis[6], George Kakavelakis[8,*], Essa A. Alharbi[1,*].

[1] Microelectronics and Semiconductor Institute, King Abdulaziz City for Science and Technology (KACST),Riyadh, 11442, Saudi Arabia

[2] Sustainable Energy Technologies Center, College of Engineering, King Saud University, Riyadh, Saudi Arabia

[3] Institute of Electronic Structure and Laser (IESL), Foundation for Research and Technology – Hellas (FORTH), 70013 Heraklion, Crete, Greece

[4] Energy, Industry, and Advanced Technologies Research Center, Taibah University, Madinah, Saudi Arabia

[5] Department of Electrical Engineering, College of Engineering, Taibah University, Madinah, Saudi Arabia.

[6] Department of Electrical & Computer Engineering, Hellenic Mediterranean University (HMU), Heraklion 71410, Crete, Greece.

[7] Physics and Astronomy Department, College of Science, King Saud University, Riyadh 11451, Saudi Arabia.

[8] Department of Electronic Engineering, School of Engineering, Hellenic Mediterranean University, Romanou 3, Chalepa, Chania, Crete GR-73100, Greece

[9] Department of Materials Science and Engineering, University of Crete, 70013 Heraklion, Crete, Greece

[10] King Abdullah Institute for Nanotechnology, King Saud University, Riyadh 11451, Saudi Arabia.

[+]These authors contributed equally to this work.

*Corresponding authors: ealharbi@kacst.gov.sa and kakavelakis@hmu.gr

Optical-Electrical Modeling

The *J–V* characteristics and photovoltaic (PV) parameters (V_{OC}, J_{SC}, FF, and PCE) of the examined perovskite-based solar cells (PSCs) were simulated using optical full-wave electromagnetic simulations and electrical drift–diffusion modelling based on the Finite Element Method.[72]

Optical simulations were performed by numerically solving Maxwell's equations in the frequency domain to compute the total electric field vector $\boldsymbol{E}(z, \nu)$ at each position z in the PSC and at each frequency ν. From $\boldsymbol{E}(z, \nu)$, the spectral absorbed energy density $Q(z, \nu)$ in the photoactive layer is calculated as:[81]

$$Q(z,\nu) = \frac{1}{2} c\varepsilon_0 \alpha(\nu) n(\nu) E(z,\nu)^2, \quad (1)$$

where c is the vacuum speed of light, ε_0 is the vacuum permittivity, $\alpha = 2\pi\kappa/\lambda$ is the absorption coefficient, with n and κ representing the refractive index and extinction coefficient (i.e., real and imaginary part of the complex refractive index) of the photoactive layer, respectively. The absorbed energy density $Q(z, \nu)$ is then used to determine the spatially resolved spectral electron-hole generation rate $G(z, \nu)$:[81,82]

$$G(z,\nu) = \frac{Q(z,\nu)}{h\nu} = \frac{\pi\varepsilon'' \varepsilon_0}{h} E(z,\nu)^2, \quad (2)$$

where h is Planck's constant and ε'' (=$2nk$) is the imaginary part of the permittivity of the photoactive layer. The total spatially resolved generation rate $G(z)$ is obtained by integrating $G(z, \nu)$ over frequency ν, weighted by the WLED illumination spectrum

$I_{WLED}(\nu)$, corresponding to various color temperatures (CTs) and intensities (see Figure S2):[73–76,81,83]

$$G(z) = \int G(z,\nu) I_{WLED}(\nu) d\nu, \quad (3)$$

Based on $G(z)$, electrical simulations were performed by numerically solving the steady-state Poisson and continuity equations to obtain the electron and hole current densities. For the one-dimensional (1D) case, these equations are explicitly given by:[74–76,83]

$$\frac{d^2\psi(z)}{dz^2} = \frac{q}{\varepsilon_0 \varepsilon_r}\left(n(z) - p(z) + N_A - N_D\right), \quad (4)$$

$$\frac{1}{q}\frac{dJ_n}{dz} + G(z) - U(z) = 0, \quad (5)$$

$$\frac{1}{q}\frac{dJ_p}{dz} + U(z) - G(z) = 0, \quad (6)$$

where ψ is the electrostatic potential, q is the elementary charge, ε_0 and ε_r are the vacuum and relative permittivity, n and p are electron and hole concentrations, N_A and N_D are the acceptor and donor doping concentrations, and J_n and J_p are the electron and hole current densities, respectively, described by the drift–diffusion constitutive relations.[73,74,76,83] In eqs 5 and 6, $G(z)$ is the generation rate (see eq 3), and $U(z)$ is the recombination rate, modeled using Shockley–Read–Hall (SRH) nonradiative trap-assisted recombination assuming equal carrier lifetimes for electrons and holes.[73,74,83]

The device architecture used in this study is FTO/TiO_2/$Cs_xFA_{x\text{-}1}Pb(I_{1-y}Br_y)_3$/Spiro-OMeTAD/Au (see also Figure 2a–c), where fluorine-doped tin oxide (FTO) and gold (Au) serve as the transparent and metal electrodes, respectively. Titanium dioxide (TiO_2) and

Spiro-OMeTAD form the electron-transporting layer (ETL) and hole-transporting layer (HTL), respectively. $Cs_xFA_{x-1}Pb(I_{1-y}Br_y)_3$ is the photoactive perovskite layer. The complex refractive indices of perovskites films with different bandgaps were obtained from refs 84–86. Material parameters used in the electrical simulations are listed in Table S1 and correspond to typical indoor PSC operation conditions.[75–78,83] Electron-hole carrier lifetimes for each bandgap were calibrated against experimental data to ensure accurate simulation results.[75,77,78] The optical-electrical model was calibrated under 3000 K and 1000 lux WLED illumination for the three specific bandgaps: 1.55, 1.72, and 1.88 eV. Finally, the calibrated PSCs were evaluated under different WLED CTs (3000, 4000, and 5500 K) and varying illumination intensities (1000, 500, and 250 lux).

Table S1. Material parameters used in the device simulations, where CB and CB are the conduction and valence band, respectively.[75–78,83]

Parameters	TiO_2	$Cs_xFA_{x-1}Pb(I_{1-y}Br_y)_3$	Spiro-OMeTAD
Thickness (nm)	200	100–1000	200
Bandgap (eV)	3	1.55–1.85	3
Electron affinity (eV)	4	3.9	2.35
Dielectric permittivity	10	6.5	3
CB density of states (cm^{-3})	1×10^{20}	1.8×10^{18}	2.2×10^{18}
VB density of states (cm^{-3})	1×10^{20}	1.8×10^{18}	1.8×10^{19}
Electron mobility ($cm^2/V\cdot s$)	20	2	2×10^{-4}
Hole mobility ($cm^2/V\cdot s$)	10	2	2×10^{-4}
Shallow uniform donor density (cm^{-3})	1×10^{18}	0	0
Shallow uniform acceptor density (cm^{-3})	0	1×10^{14}	2×10^{18}
Electron lifetime (ns)	5	20–55	5
Hole lifetime (ns)	5	20–55	5

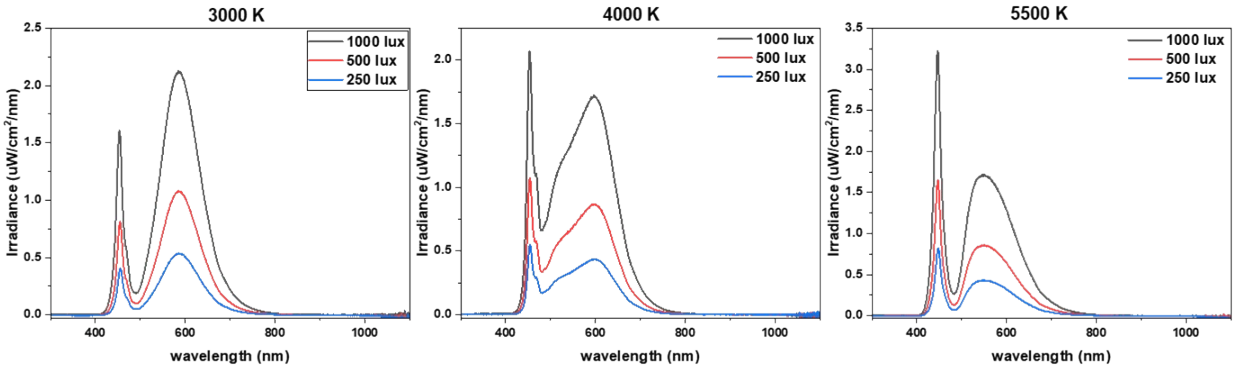

Figure S1. Spectrum of WLED with various color temperatures (see titles) and intensities (see legends).

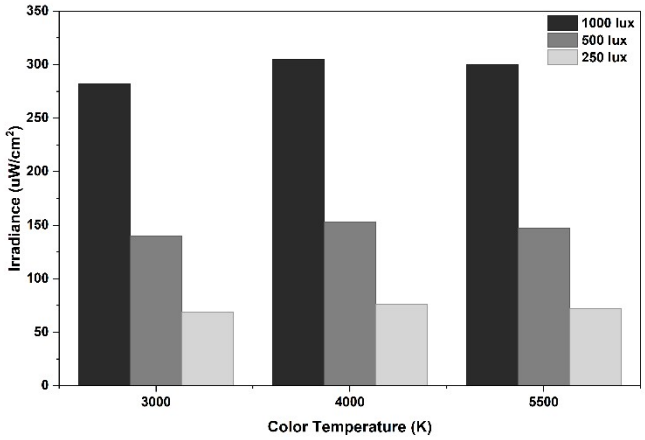

Figure S2. Irradiance levels under different color temperatures (3000 K, 4000 K, 5500 K) at various illuminance conditions (1000, 500, and 250 lux).

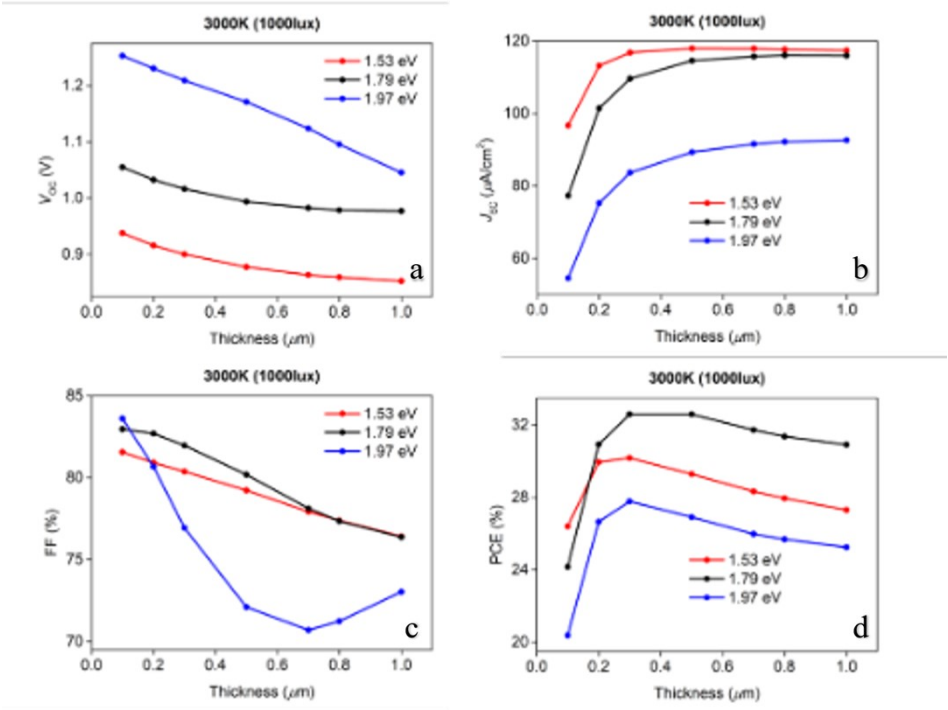

Figure S3. Simulation of photovoltaic parameters (*Voc*, *Jsc*, FF, and PCE) for perovskite solar cells with varying bandgaps as a function of perovskite layer thickness under 3000 K and 1000 lux illumination.

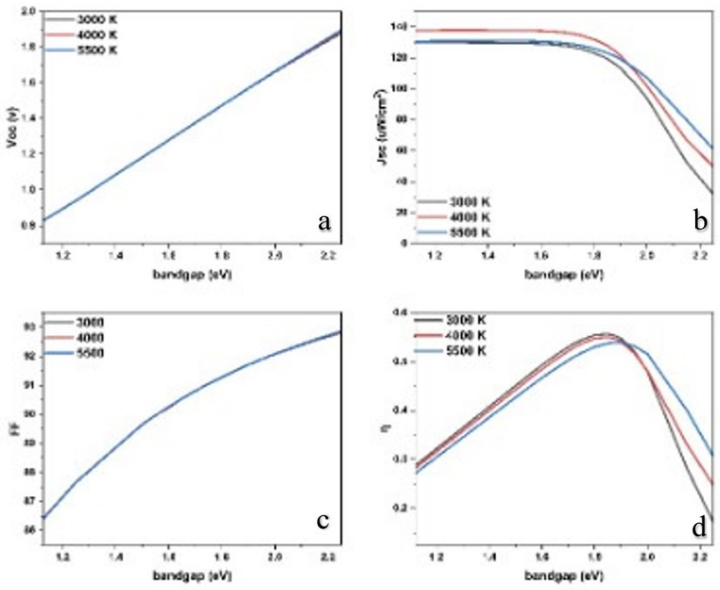

Figure S4. Theoretical SQ limit analysis of solar cell performance under WLED with various color temperatures.

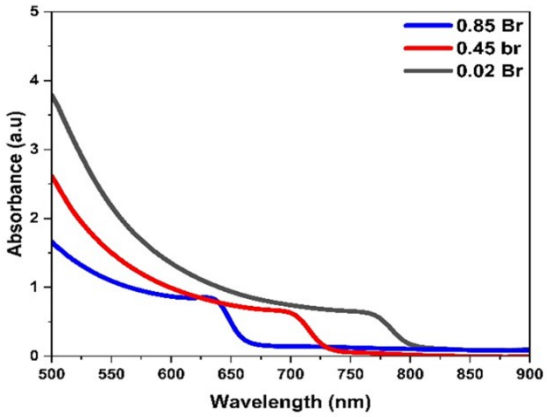

Figure S5. UV-vis of perovskite films.

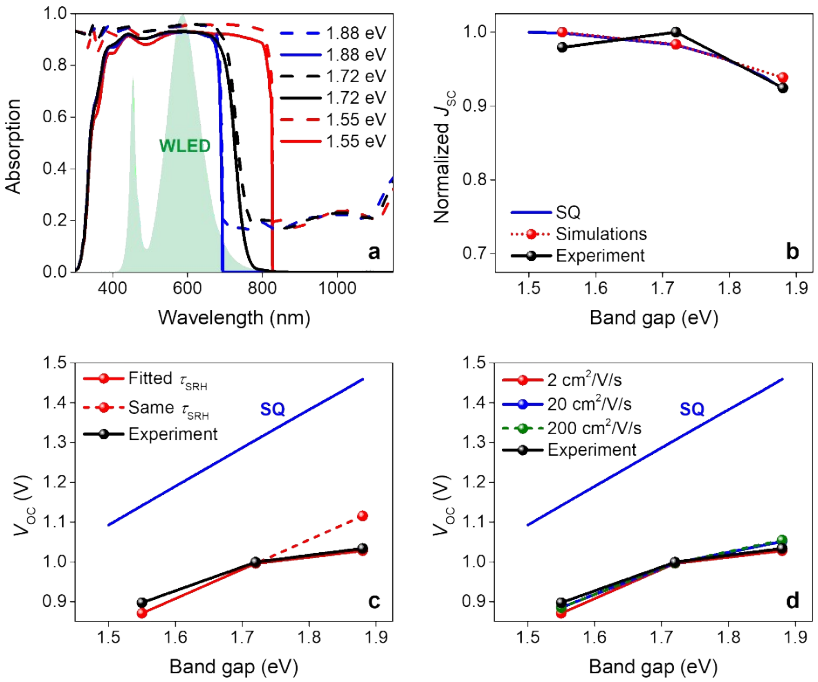

Figure S6. (a) Simulated total absorption spectra (dashed) and within perovskite layer (solid) for the examined band gap cases of 1.88 eV (blue), 1.72 eV (black), and 1.55 eV (red), along with the normalized WLED spectrum (3000 K). (b) Experimental (black) and simulated (red) normalized J_{SC} as a function of perovskite band gap compared with SQ limit calculations (blue), showing similar trends. . (c) Experimental (solid black) and simulated (solid red) V_{OC} as a function of perovskite band gap compared with SQ limit calculations (solid blue) and simulations assuming equal carrier lifetimes for all band gap cases (dashed red), showing lower V_{OC} deficits for the 1.55 and 1.72 eV band gap cases. (d) Simulated normalized V_{OC} as a function of perovskite band gap assuming varying

electron-hole carrier mobilities (2, 20, 200 $cm^2\ V^{-1}\ s^{-1}$), showing no substantial effect on V_{OC}

Table S2. Performance of the 1.55 eV devices for different precursor concentrations.

Precursor concentration (M)	*Voc* (V)	PCE (%)	Fill Factor (%)	*Jsc* ($\mu A/cm^2$)
0.9	0.831	25.85	76.15	114.8
1.1	0.837	27.07	73.83	123.1
1.2	0.854	26.98	72.05	122.8
1.3	0.897	30.05	76.73	121.4
1.4	0.802	29.46	78.99	130.2

Table S3. Performance table of the 1.55 eV devices across different color temperatures and intensities.

K/Lux	*Voc* (V)	PCE (%)	Fill Factor (%)	*Jsc* ($\mu A/cm^2$)
3000-1000	0.897	30.05	76.73	121.365
3000-500	0.852	29.91	77.92	61.568
3000-250	0.819	31.29	79.72	32.000
4000-1000	0.903	28.81	75.03	128.127
4000-500	0.858	28.28	75.73	65.081
4000-250	0.828	29.30	77.27	34.601
5500-1000	0.904	28.72	76.74	122.765
5500-500	0.857	28.11	77.16	62.619
5500-250	0.825	29.47	79.23	32.944

Table S4. Performance table of the 1.72 eV devices across different color temperatures and intensities.

K/Lux	*Voc* (V)	PCE (%)	Fill Factor (%)	*Jsc* (μA/cm^2)
3000-1000	0.999	35.04	78.54	123.943
3000-500	0.962	34.61	77.42	64.373
3000-250	0.924	36.59	78.46	34.262
4000-1000	1.006	34.10	78.17	132.107
4000-500	0.967	33.51	77.56	68.134
4000-250	0.924	34.27	78.44	36.448
5500-1000	0.992	32.22	74.60	129.452
5500-500	0.957	34.01	78.24	66.094
5500-250	0.924	36.61	77.93	35.505

Table S5. Performance table of the 1.88 eV devices across different color temperatures and intensities.

K/Lux	*Voc* (V)	PCE (%)	Fill Factor (%)	*Jsc* (μA/cm^2)
3000-1000	1.034	29.20	68.54	114.56
3000-500	0.998	32.19	70.82	62.30
3000-250	0.963	36.65	74.95	33.66
4000-1000	1.043	29.31	67.45	126.09
4000-500	1.004	31.75	70.65	67.14
4000-250	0.976	36.29	73.02	37.55
5500-1000	1.044	29.72	68.11	124.63
5500-500	1.006	32.33	70.66	66.93
5500-250	0.969	37.44	71.78	39.09